Mon. Not. R. astr. Soc. (1986) **223**, 151–172

The determination of the mass of a Magellanic Cloud planetary nebula by speckle interferometry

M. J. Barlow *Department of Physics and Astronomy, University College London, Gower Street, London WC1E 6BT*

B. L. Morgan, C. Standley and H. Vine *Blackett Laboratory, Imperial College of Science and Technology, Prince Consort Road, London SW7 2BZ*

Accepted 1986 May 28. Received 1986 May 28; in original form 1985 August 12

Summary. We have resolved a Magellanic Cloud planetary nebula by speckle interferometry for the first time. Our observations of SMC N2 show it to have a double-ring structure, the rings having angular radii of 0.22 and 0.38 arcsec, corresponding to absolute radii of 0.06 and 0.10 pc. Our speckle observations of the galactic planetary nebula Vy 2−2 show a ring of angular diameter 0.4 arcsec, in agreement with previous VLA radio data. We have determined the radial hydrogen density profile for SMC N2 and have derived masses of $0.09\,M_{\odot}$ and $0.27\,M_{\odot}$ for the inner and outer shells respectively, so that the total mass of this optically thin nebula is $0.36\,M_{\odot}$. The nebular expansion velocity of SMC N2 has been derived from a high-resolution spectrum of the [O III] 5007 Å line and expansion ages of between 5000 and 12 000 yr have been derived for the shells. A reanalysis of the available nebular data leads us to derive a central star effective temperature of 110 000 K and a luminosity of $4340\,L_{\odot}$, corresponding to a stellar mass of $0.59\,M_{\odot}$, from a comparison with published evolutionary tracks. The stellar evolutionary age since leaving the AGB is about 8000 yr, consistent with the nebular expansion age.

1 Introduction

The masses of planetary nebula shells are of interest for at least three distinct reasons. (i) A knowledge of the shell masses can allow a quantification of the contribution which is made to the recycling and chemical enrichment of the interstellar medium by the low-to intermediate-mass stars which are responsible for planetary nebulae (PN). (ii) The central stars of PN evolve to become white dwarfs. Since the masses of central stars can be determined by fitting theoretical evolutionary tracks through their observed L, $T_{\rm eff}$ positions in the H–R diagram, the determination of nebular masses will allow the masses of white dwarfs to be linked to those of the progenitor asymptotic giant branch (AGB) stars. With a subsequent understanding of the mass-loss processes which occur prior to the planetary nebula formation stage of AGB stars, the

masses of white dwarfs may eventually be linked back to the original main-sequence stellar masses. (iii) The physical processes responsible for planetary nebula formation are of interest in their own right. A determination of the masses of planetary nebula shells as a function of stellar core mass may help to diagnose the PN ejection mechanism itself.

In order to derive the mass of a planetary nebula, one needs to determine the ion number density as a function of absolute radius. This requires that the nebula be well resolved and that its distance be accurately known. The first requirement is satisfied by PN in our own Galaxy but unfortunately their distances are usually uncertain by at least 50 per cent (see Gathier *et al.* 1983) because no good intrinsic calibrator exists. To illustrate the effect of this degree of distance uncertainty on mass determinations, consider a PN at distance D, with absolute radius R, mean ion density n, and a filling factor ε, where ε is the fraction of the nebular volume which is occupied by ions of mean density n. The mass of the PN, $M(\mathrm{PN})$, is proportional to $\varepsilon n\theta^3 D^3$, where $\theta = R/D$ is the nebular angular radius. The observed Hβ flux, by recombination theory, is proportional to $\varepsilon n^2 R^3/D^2$, or $\varepsilon n^2\theta^3 D$. For a nebula with a measured angular radius and Hβ flux we have $n \propto (\varepsilon D)^{-1/2}$, so that we obtain $M(\mathrm{PN}) \propto \varepsilon^{1/2} D^{5/2}$. If the value of n is known independently, then, since $\varepsilon \propto 1/n^2 D$, we obtain $M(\mathrm{PN}) \propto D^2/n$. Thus a 50 per cent uncertainty in D translates into a factor of 2.3 uncertainty in $M(\mathrm{PN})$.

Gathier *et al.* (1983) have carried out a radio interferometric study of PN in the direction of the central bulge region of our Galaxy and have derived the nebular masses from their measured radio fluxes and diameters, under the assumption that they had filling factors of unity and that they were close to the Galactic Centre, for which a distance of 9 kpc was adopted. However, the PN towards the Galactic Centre are heavily obscured and so their properties are difficult to study at other wavelengths.

The PN in the Magellanic Clouds are very lightly obscured, and so their spectroscopic properties are relatively easy to study. Their distances are known relatively accurately because of the existence of a sufficient number of independent distance calibrators in each galaxy. A likely distance modulus uncertainty of 0.3 mag translates into an uncertainty of only 30 per cent in the derived nebular masses. However, good angular diameter estimates are required. Standard imaging techniques have only managed to resolve about half a dozen relatively old and faint PN in the Magellanic Clouds (Jacoby 1980), and the majority of the currently known PN are expected to have angular diameters of <1 arcsec (see Webster 1969, 1976). Although spaceborne imaging will undoubtedly be of benefit for the study of Magellanic Cloud PN, we will show that the use of standard speckle interferometric techniques at the 3.9-m Anglo–Australian Telescope has allowed us to derive angular diameters, radial brightness distributions and nebular masses for these objects. We present here our first speckle observations to resolve a Magellanic Cloud planetary nebula, SMC N2, obtained on 1983 November 18 when weather conditions only permitted observations of this PN. A second observing run in 1984 October yielded speckle interferometric data on 20 more Magellanic Cloud PN and those data will be described in a subsequent publication. As a check on our techniques, we also obtained speckle observations in 1984 October of the bright compact galactic PN Vy 2−2, whose subarcsec structure had been previously determined at VLA radio wavelengths (Seaquist & Davis 1983). Our observations and analysis of Vy 2−2 are included in Section 3.

2 Observations

The Imperial College speckle interferometer was operated in photon counting mode at the $f/15$ focus of the 3.9-m Anglo-Australian Telescope. The results were analysed with a hard-wired autocorrelator. A detailed description of these instruments is given by Hebden, Morgan & Vine (1983). A 75-mm objective was used for the observations of SMC N2, yielding a 4.6-arcsec field of

view and a pixel size of 0.018 arcsec. With this plate-scale, the maximum observable structural separation corresponds to about 1.1 arcsec, while the limit to the smallest measurable structural separation is determined by the width of the central photon spike in the autocorrelation plot; this spike corresponds to vectors between pixels within the same photon event. At the plate-scale used here, the base radius of the photon spike was about 0.14 arcsec.

We imaged through a 50 Å bandpass filter centred on the [O III] 5007 Å line. This filter was chosen because: (i) the narrow filter strongly suppresses the dense Magellanic Cloud stellar background and background photons from the moonlit sky. (ii) The [O III] 5007 Å line is usually the strongest line emitted by PN. Its strength is typically 10 times that of Hβ, allowing nebulae to be speckled which are too faint for Hβ observations. (iii) Ionization structure models of PN predict (e.g. figs 2.5 and 2.6 of Osterbrock 1974), and images of galactic PN confirm (e.g. Atherton *et al.* 1978), that the brightness distribution of a PN in the [O III] line is very similar to that in the Hβ line, for central star temperatures in excess of about 40 000 K. This encompasses the majority of PN. Nebulae with central star temperatures below this value can be easily recognized by their low-excitation spectra. Confirming this, our speckle data for the galactic PN Vy 2−2 (Section 3) show near agreement between the [O III] and Hβ structures.

In the selection of PN, it is important to choose objects which are likely to be optically thin in the hydrogen Lyman continuum, in order that the ionized nebular mass be equal to the total mass of the ejected shell. The best indicator of this is if the stellar He II Zanstra temperature is significantly larger than the H I Zanstra temperature but, in the absence of data on the central star, other selection criteria can be utilized, such as the presence of relatively weak lines from low ion stages. In general we preferred the lower density (n_e<5000 cm^{-3}) and/or the high-excitation PN, since by evolutionary arguments these are more likely to be optically thin. We chose to observe SMC N2 (Henize 1956) because of the very high luminosity, $3\times10^4\,L_\odot$, that had been derived for its central star by Stecher *et al.* (1982). However, as will be seen in Section 6 and in the Appendix, our reanalysis of the available data leads us to derive a much lower stellar luminosity.

SMC N2 was imaged in the [O III] line for 60 min at a frame-rate of 25 Hz. Two-dimensional spatial autocorrelations over all azimuthal angles were produced between all pixel events on each frame and the results were summed to yield the dotted plot in Fig. 1(a). This plot can be seen to exhibit significant structure, most noticeably three broad peaks, corresponding to vectors between points separated by 12 pixels (0.22 arcsec), 23 pixels (0.41 arcsec) and 32 pixels (0.59 arcsec). A nearby unresolved reference star, SAO 255683, was also observed for 30 min immediately after the SMC N2 observation, through an additional neutral density filter, and the autocorrelation plot in Fig. 1(b) was produced. In addition to the central photon spike, the autocorrelation plot for SAO 255683 exhibits the normal extended seeing pedestal, which can be approximated by a near-Gaussian fit [i.e. $\exp-(x/a)^{5/3}$, see Roddier 1981]. The slope of the outer seeing pedestal of SMC N2 in Fig. 1(a) is not the same as that of the reference star in Fig. 1(b), presumably due to changes in the seeing during the period of 2 hr over which both observations were made. A number of near-Gaussian curves [e.g. the solid line in Fig. 1(a)] were normalized to the outer part of the SMC N2 autocorrelation and then subtracted to yield the speckle component. While the resulting speckle components [e.g. the dashed curve in Fig. 1(a)] thus showed different absolute amplitudes at the peaks, the positions of the peaks were of course invariant and the relative amplitudes of the peaks (which along with the positions are modelled in Section 3) varied much more slowly than their absolute levels.

In order to investigate the significance of the peaks and troughs present in the SMC N2 autocorrelation shown in Fig. 1(a), we also fitted a near-Gaussian to the dotted points and then compared the positive and negative excursions from this near-Gaussian, at separations larger than 0.2 arcsec, with the deviations expected on the basis of counting statistics alone. The ratio of the observed to expected deviations was found to range up to 25 for SMC N2, whereas for the case

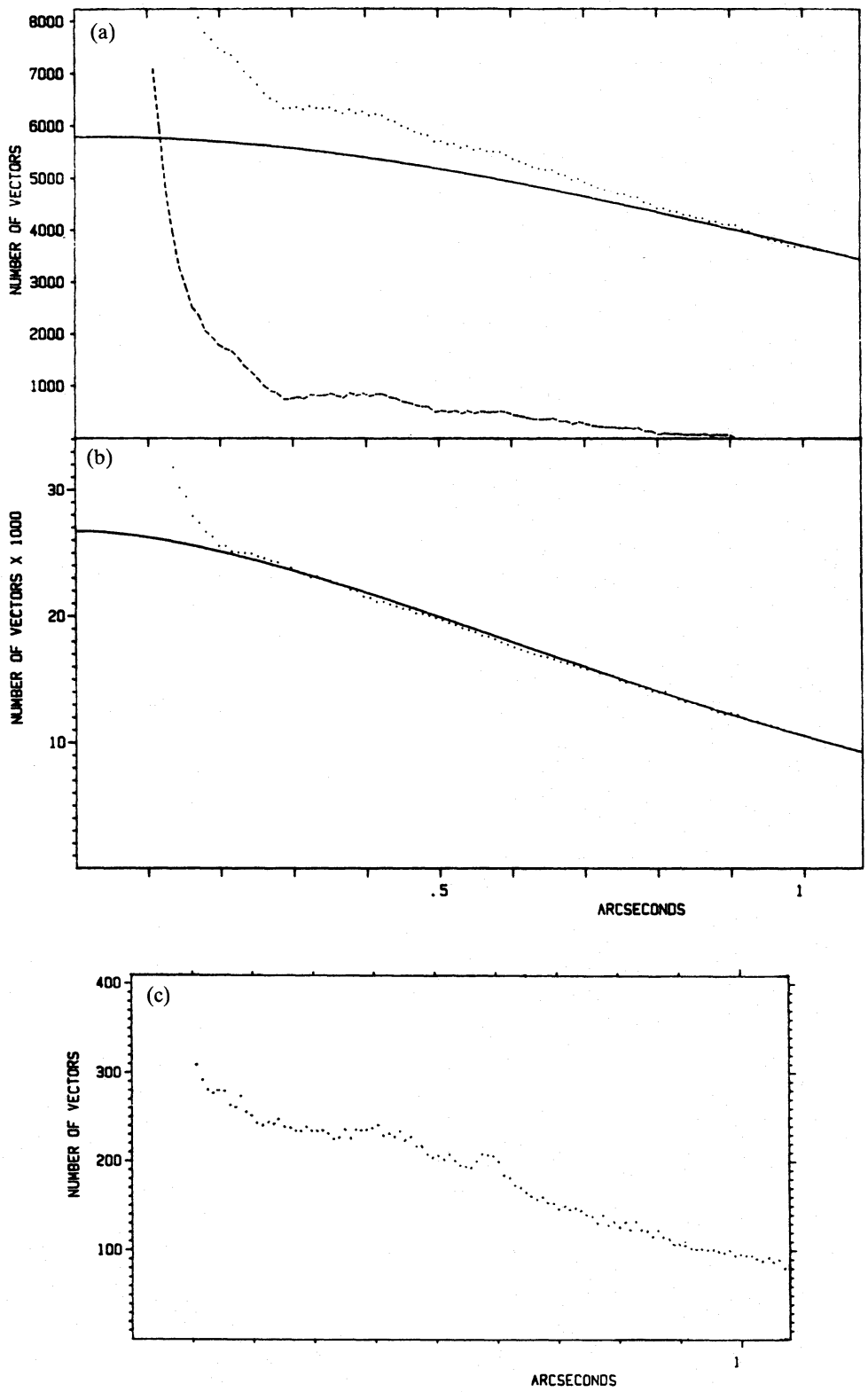

Figure 1. (a) and (b) The dotted plot in (a) (upper) shows the mean autocorrelation of a 60 min observation, made in 1983 November, of SMC N2 in the [O III] line. The dotted plot in (b) (lower) shows the mean autocorrelation of a 30 min observation, made through a neutral density filter and [O III] filter, of the nearby unresolved reference star SAO 255683. The solid curve in (b) is a near-Gaussian fit (see text) to the seeing pedestal of the SAO 255683 autocorrelation plot. The solid curve in (a), which is also a near-Gaussian fit to the seeing pedestal, has been normalized at 0.9 and 1.01 arcsec to the SMC N2 autocorrelation and subtracted to yield the speckle component, shown as a dashed curve in (a). (c) The mean autocorrelation of a 6 min observation of SMC N2 in the [O III] line, made in 1984 October.

of the near-Gaussian fitted to the reference star autocorrelation in Fig. 1(b), the ratio of observed to expected deviations did not exceed 10.

During our 1984 October AAT observing run, SMC N2 was reobserved with the same instrumental set-up as described above but, due to a recording equipment failure, only 6 min of useful data were obtained. Fig. 1(c) shows the resulting autocorrelation. Although the overall signal is much lower than for the 1983 data shown in Fig. 1(a), the peaks at 0.41 and 0.59 arcsec in the 1983 data can be clearly seen in the 1984 data as well.

3 Autocorrelation models

The presence of more than one peak in the autocorrelation function for SMC N2 suggests the presence of more than one peak in its brightness distribution. In order to model the intrinsic brightness distribution, we assumed azimuthal symmetry for SMC N2. The total number of counts which we obtained prevents us making detailed statements about the degree of symmetry.

Our approach was to autocorrelate a range of azimuthally symmetric input-model angular brightness distributions over all azimuthal angles and to compare the resulting plots with the speckle component in Fig. 1(a). Uniform, edge-brightened, or centrally peaked discs were found not to yield autocorrelation functions which resembled it in any way. Since many galactic PN exhibit ring structure, we therefore experimented with models having such peaks in their radial brightness distributions. We found it convenient to construct the distributions using functions of the type described by Harrington & Feibelman (1983). The angular intensity distribution of the best-fitting azimuthally symmetric model is shown in Fig. 2(a) and its autocorrelation is shown in Fig. 2(b), along with the observed speckle component. The model has a double-ring structure, with peaks at angular distances of 0.22 and 0.38 arcsec from the centre. The positions of the peaks in the autocorrelation plot are sensitive to the separation of the peaks in the radial-intensity model, allowing the positions of the latter to be determined to ± 1 pixel (± 0.018 arcsec). The feature at 0.22 arcsec in the autocorrelation plot corresponds to vectors between points on the inner ring and points on the outer ring at the same side of the nebula. The feature at 0.41 arcsec corresponds to vectors between points on the inner ring which are at opposite sides of the nebula, while the feature at 0.59 arcsec corresponds to vectors between points on the inner ring and points on the outer ring which are at opposite sides of the nebula. The position of the first autocorrelation peak is redundantly specified by the positions of the second and third peaks and its presence provides a valuable confirmation of the validity of the model. A fourth peak is expected to be present at about 0.76 arcsec, corresponding to vectors between points on the outer ring at opposite sides of the nebula, but our signal is too low at that separation to easily reveal it.

The relative strengths of the two peaks in the model intensity distribution determines the contrast of the features in the autocorrelation. A decrease in the relative intensity of the outer ring leads to a reduction in the contrast of the autocorrelation features at 0.22 and 0.59 arcsec, while an increase in the relative intensity of the outer ring causes them to become increasingly prominent relative to the feature at 0.41 arcsec. The closest fit to the observed contrast of the autocorrelation features was obtained with a double-ring model with an intensity ratio of 3:1 at the peaks [Fig. 2(a)].

The formulation of Harrington & Feibelman (1983) predicts a certain degree of central infilling for the projected intensity distribution of any spherically symmetric shell-like PN, due to the projection of emission from the outer regions on to the centre. However, we are able to set an upper limit to the brightness of any central infilling in SMC N2 of less than 20 per cent of the intensity at the peak of the inner ring, since any central infilling will contribute vectors which will tend to wash out the contrast of the features which correspond to vectors between the intensity peaks. In this respect, SMC N2 appears to resemble galactic PN such as the Ring Nebula NGC

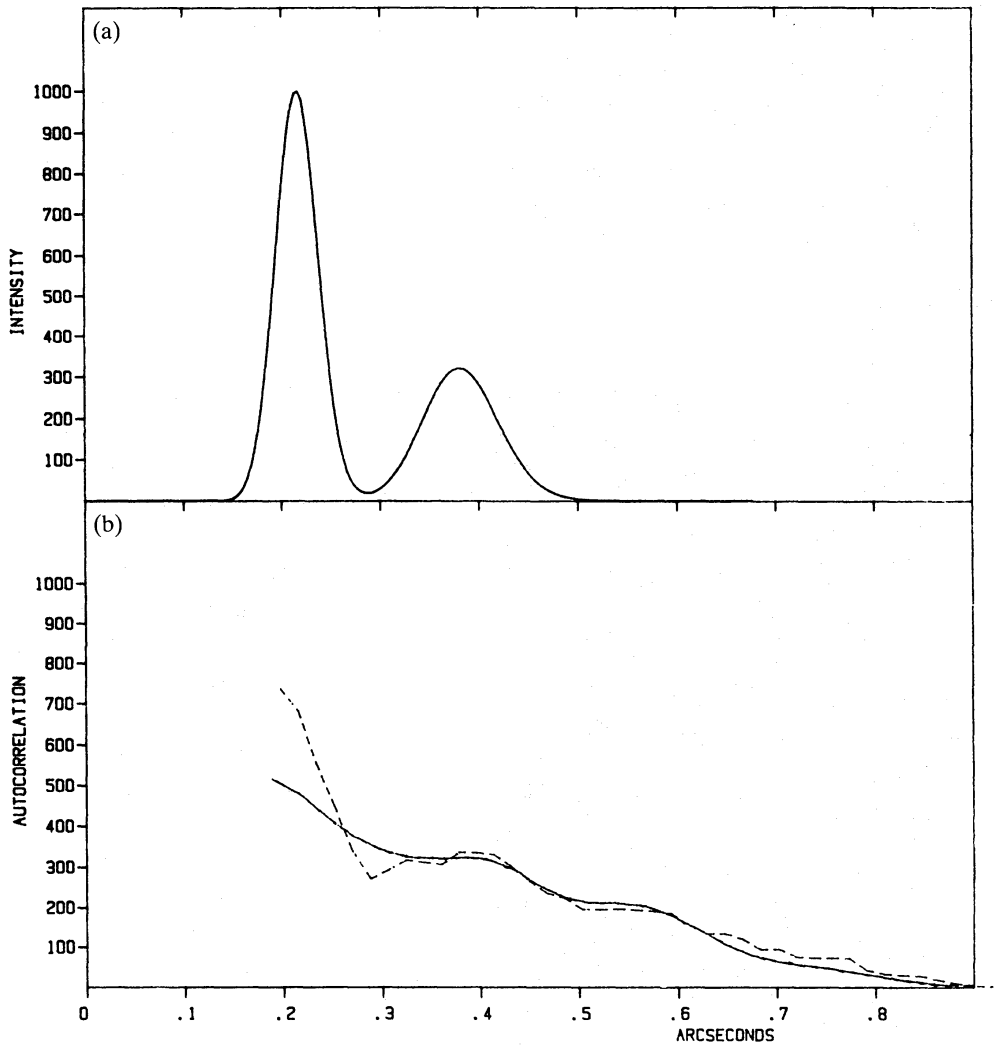

Figure 2. (a) (upper) shows the best-fitting model angular intensity distribution for SMC N2 in the [O III] line, the autocorrelation of which yields the solid curve in (b) (lower). For comparison, the speckle component of SMC N2 [dashed plot in (b)] has been normalized to the model autocorrelation at a separation of 0.36 arcsec. The observed speckle component and the model autocorrelation are not plotted for separations less than 0.2 arcsec, because of the presence of the central photon spike in the former.

6720 (Atherton *et al.* 1978), which also exhibit a very low degree of central infilling. A toroidal structure, rather than a spherical shell, seen in projection, as assumed here, might provide an explanation for this behaviour. In converting our derived azimuthally symmetric angular intensity distribution into a spherically symmetric radial-density distribution (Section 4), we have assumed that Fig. 2(a) gives a good fit to the spherically symmetric radial emissivity distribution of the nebula as well as to the projected angular brightness distribution. Since the predicted differences between these two functions occur mainly in the central region (see fig. 5 of Harrington & Feibelman 1983), where little mass is contained, this seems a reasonable assumption.

In order to further confirm the validity of our modelling procedure, it appeared useful to us to obtain speckle observations of a compact PN whose subarcsec brightness distribution had been independently determined by other means. Very few such objects exist, but fortunately the VLA radio study of the galactic PN Vy 2−2, by Seaquist & Davis (1983), showed it to be a suitable comparison object. Their 15-GHz radio map shows Vy 2−2 to be dominated by a symmetric

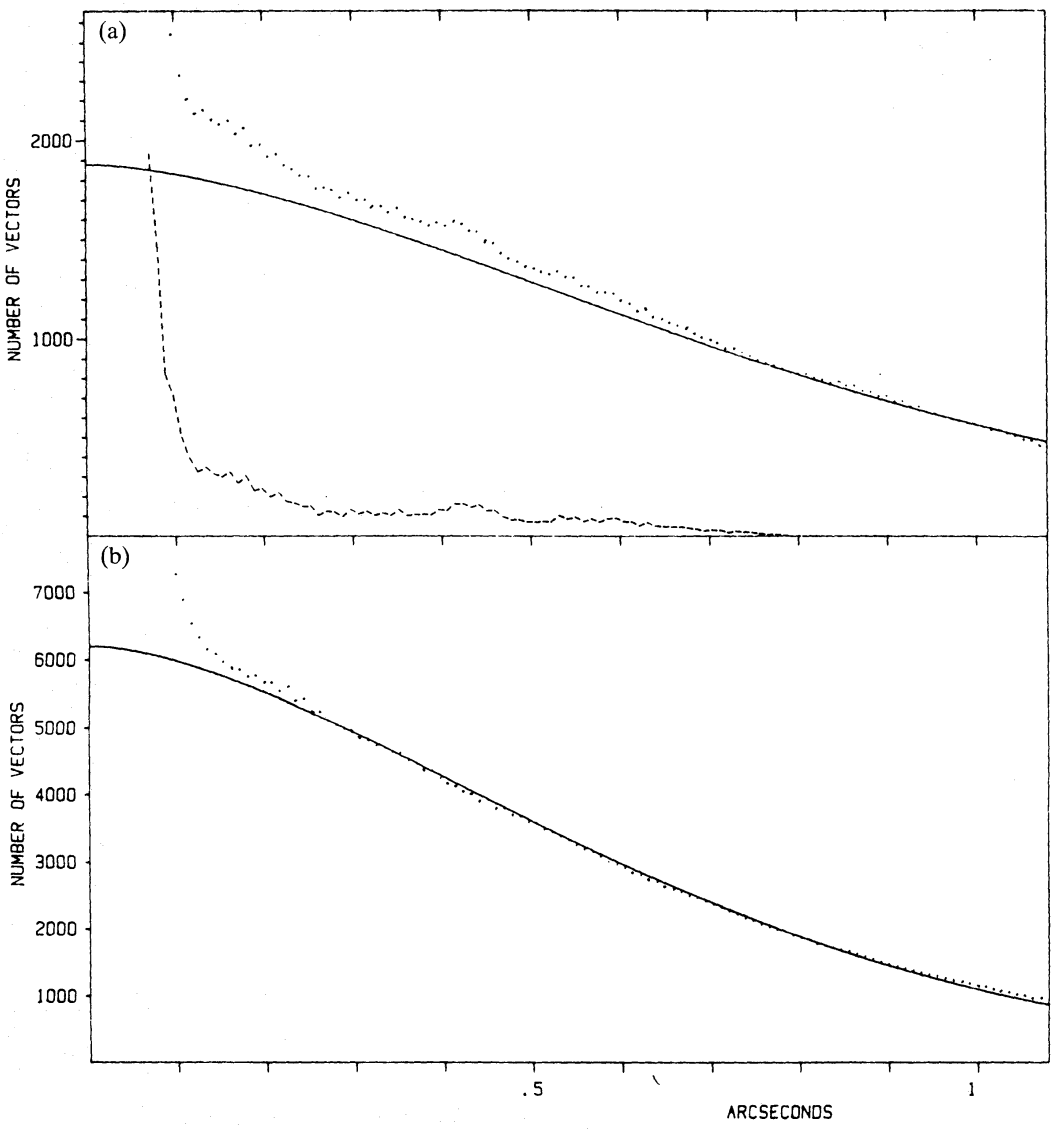

Figure 3. As for Fig. 1, but for an 11 min Hβ observation of Vy 2−2, shown as the dotted plot in (a) (upper); and for a 6 min Hβ observation of the nearby unresolved reference star SAO 104799, shown in (b) (lower). The fit to the seeing pedestal in (a) (solid curve) has been normalized to the mean autocorrelation of the observations at 0.79 and 1.00 arcsec and subtracted to yield the speckle component [dashed plot in (a)].

single-ring structure, with the peak of its intensity distribution at an angular radius of about 0.2 arcsec. Such a structure should give rise to a speckle interferometric autocorrelation plot with a single peak at about 0.4 arcsec, corresponding to vectors between points on the ring at opposite sides of the nebula. Since the VLA radio flux is due to hydrogen free–free emission, the Hβ brightness profile should be the same as that found in the radio, provided no differential reddening exists across the face of the nebula. Following our arguments in Section 2, the [O III] brightness distribution should also be similar to that of Hβ. The blackbody hydrogen Zanstra temperature found by Shaw & Kaler (1985) for this optically thick PN was 41 000 K, putting it just above the minimum stellar effective temperature required for the [O III] brightness distribution to extend out to nearly the same radius as that of Hβ (Section 2).

We observed Vy 2−2 with the AAT on 1984 October 12 and 13, imaging it through the [O III] filter and through a 10 Å bandpass Hβ filter. Two different objectives were used to obtain two independent plate-scales. The dotted curve in Fig. 3(a) shows the autocorrelation of an 11-min

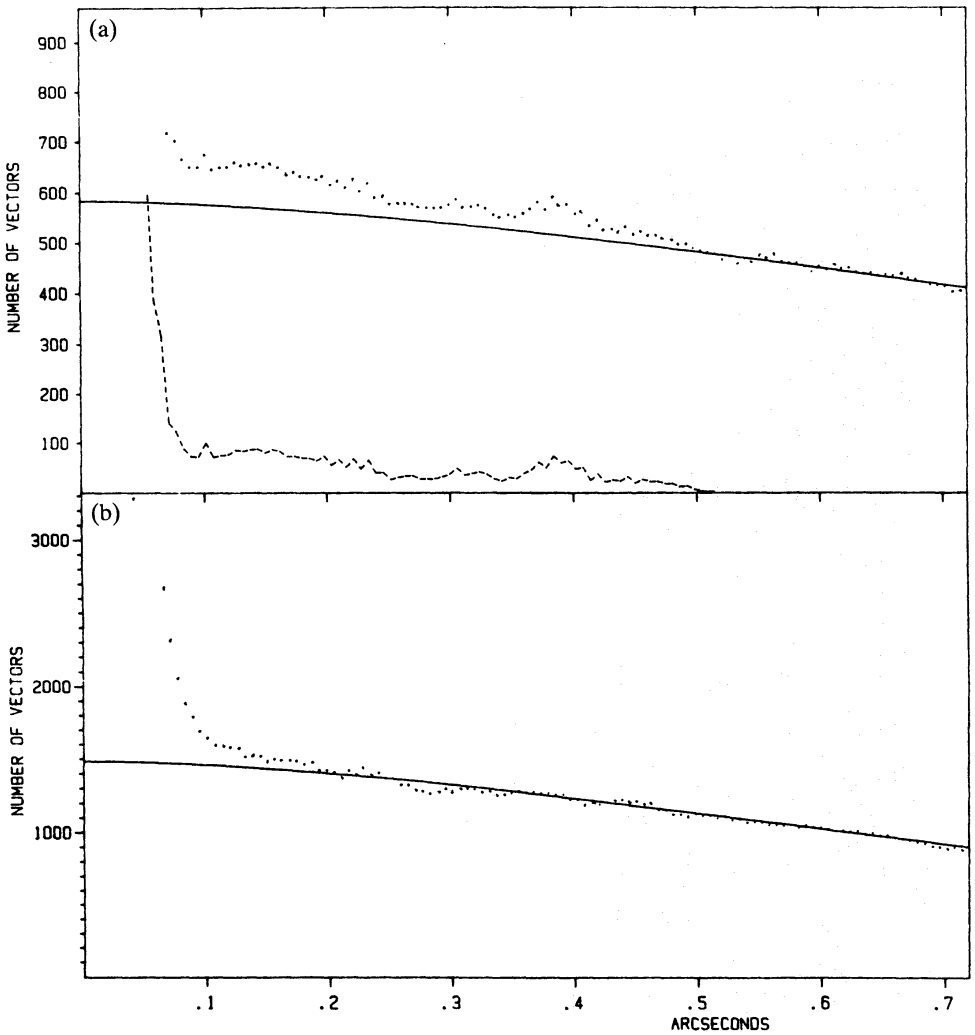

Figure 4. As for Fig. 1, but for a 6.5 min [O III] observation of Vy 2−2, shown in (a) (upper); and a 6 min [O III] observation of SAO 104799, made through a neutral density filter and shown in (b) (lower). The fit to the seeing pedestal in (a) (solid curve) has been normalized to the mean autocorrelation of the observations at 0.53 and 0.68 arcsec and subtracted to yield the speckle component [dashed plot in (a)]. These observations were made using a 50-mm objective, whereas all other observations were made using a 75-mm objective.

observation in the Hβ line using a 75-mm objective, from which we have subtracted a fit to the seeing pedestal (solid line) to yield the speckle component (dashed line). The fit to the seeing pedestal was derived from observations, made immediately afterwards, of the nearby unrevolved reference star SAO 104799 [Fig. 3(b)]. The dotted plot in Fig. 4(a) shows the autocorrelation of a 6.5-min observation of Vy 2−2 in the [O III] line using a 50-mm objective, from which we have similarly subtracted a fit to the seeing pedestal derived from the adjacent observations of SAO 104799 which are shown in Fig. 4(b). The speckle components in Figs 3(a) and 4(b) both show a feature at about 0.4 arcsec, in agreement with expectations, with the [O III] feature at a slightly smaller separation than the Hβ feature.

Model-brightness distributions have been constructed to fit the Hβ and [O III] autocorrelations and are shown in Figs 5 and 6, respectively. The [O III] speckle component can be fitted by the autocorrelation of a single azimuthally symmetric ring peaking at a radius of 0.20 arcsec, while the radius at which the model Hβ brightness distribution peaks is 0.22 arcsec. The degree of central

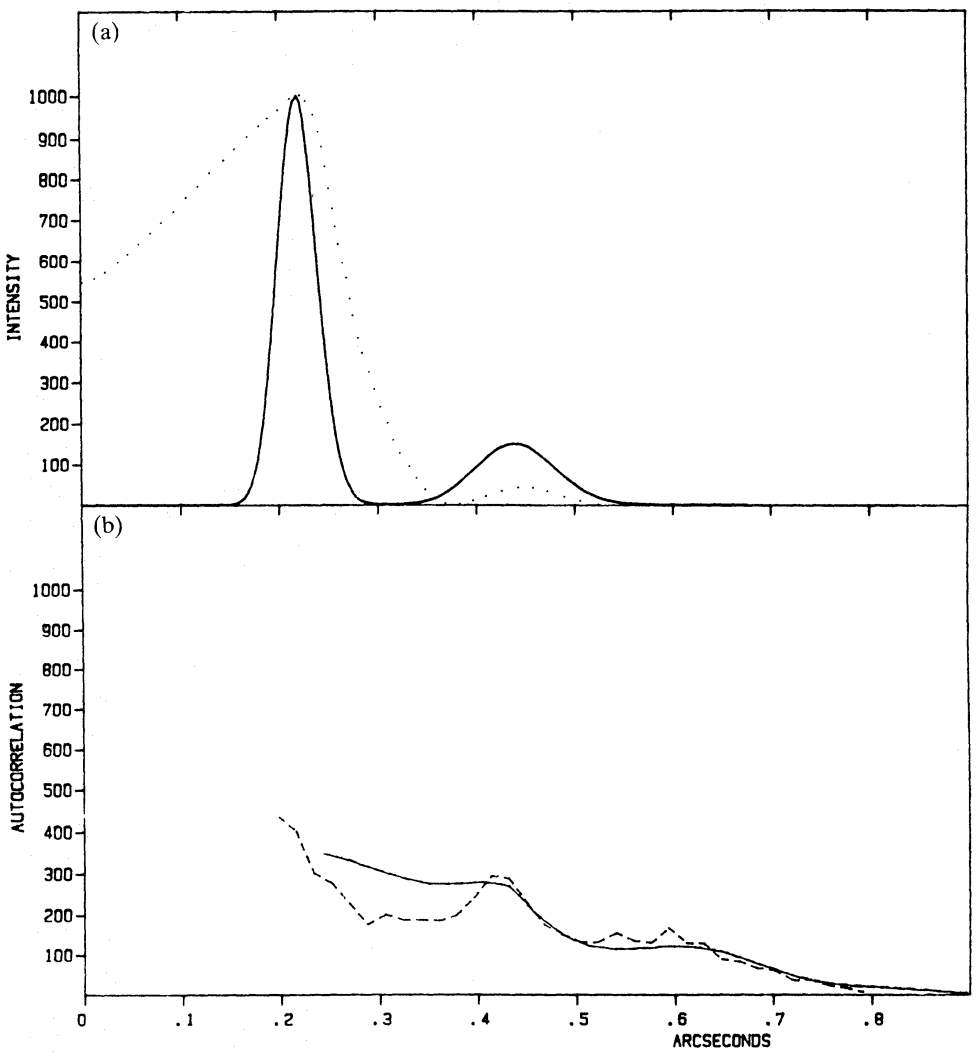

Figure 5. The solid curve in (a) (upper) is the best-fitting model angular intensity distribution for the Hβ observations of Vy 2−2. Its autocorrelation is shown by the solid curve in (b), where it is compared with the speckle component of the mean autocorrelation of the Vy 2−2 observations, shown by the dashed plot. The dotted curve in (a) shows the free–free angular brightness distribution which Seaquist & Davis (1983) derived from their 15-GHz VLA radio observations of Vy 2−2.

infilling in Hβ and [O III] is constrained by our data to be less than about 10 per cent of the peak brightness – this is significantly lower than implied by the 15-GHz radio map in fig. 3 of Seaquist & Davis (1983): the dotted curve in Fig. 5(a) shows the north–south radial brightness distribution found by the VLA. Cobb & McCarthy (1986), in a comparative study of deconvolution techniques for infrared speckle interferometry, have found that the 'CLEAN' algorithm, used for restoring VLA data, is not good for resolving closely spaced delta functions, since it tends to produce significant infilling. In other respects our model Hβ brightness distribution shows encouraging agreement with the VLA data. For example, it was found that a weak feature is present in our Hβ autocorrelation plot at a separation of about 0.6 arcsec and required a weak secondary peak in the model brightness distribution at a radius of about 0.4 arcsec [Fig. 5(a), solid curve]. This weak secondary peak is also present in the VLA cross-cut [Fig. 5(a), dotted curve], although at a lower amplitude.

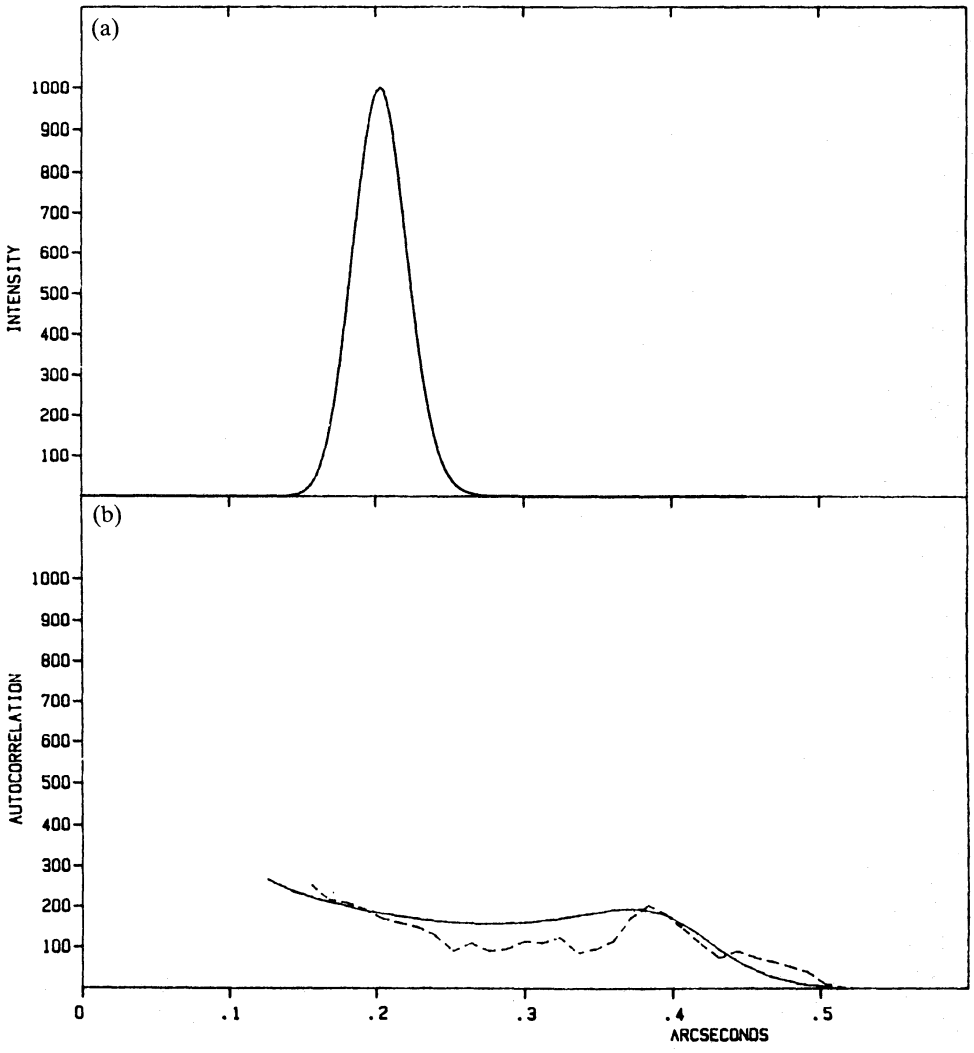

Figure 6. As for Fig. 5, but for the [O III] observations of Vy 2−2.

4 The mass of SMC N2

We shall assume that the [O III] brightness profile for SMC N2 [Fig. 2(b)] is the same as that for Hβ. Our nebular ionization structure model for SMC N2 (Appendix) shows this to be a good approximation. The volume emissivities of both [O III] and Hβ are proportional to $\varepsilon n_e n_i$, where n_e is the local electron density, n_i is the local ion density and ε is the filling factor. The total Hβ flux emitted by a nebula at distance D is given by

$$4\pi D^2 I(\mathrm{H}\beta) = \gamma \alpha_{\mathrm{eff}}(\mathrm{H}\beta) h\nu_\beta \int \varepsilon n_{\mathrm{H}}^2(r) 4\pi r^2 \, dr \qquad (1)$$

where $I(\mathrm{H}\beta)$ is the dereddened Hβ flux observed at Earth, $\alpha_{\mathrm{eff}}(\mathrm{H}\beta)$ is the partial recombination coefficient of hydrogen for the emission of Hβ photons of energy $h\nu_\beta$ (from Brocklehurst 1971), and $n_e = \gamma n(\mathrm{H}^+)$ where $\gamma = [1 + n(\mathrm{He}^+)/n(\mathrm{H}^+) + 2n(\mathrm{He}^{2+})/n(\mathrm{H}^+)]$. Similarly, $I(r)$, the line emissivity distribution as a function of radius r, is given by

$$I(r) = K\gamma \alpha_{\mathrm{eff}}(\mathrm{H}\beta) h\nu_\beta \varepsilon n_{\mathrm{H}}^2(r) \qquad (2)$$

where K is a constant. Substituting from (2) into (1) gives

$$K=[I(\mathrm{H}\beta)D^2]^{-1}\int I(r)r^2\,dr. \tag{3}$$

Using the function which generated $I(r)$ in Fig. 2(a), we can numerically evaluate $\Sigma I(r)r^2\,\Delta r$ and thereby determine the value of K using equation (3). We can then derive $n_{\mathrm{H}}(r)\sqrt{\varepsilon}$ since, by (2), we have

$$n_{\mathrm{H}}(r)\sqrt{\varepsilon}=\left[\frac{I(r)}{K\gamma\alpha_{\mathrm{eff}}(\mathrm{H}\beta)h\nu_\beta}\right]^{1/2}. \tag{4}$$

In Fig. 7 we plot $n_{\mathrm{H}}\sqrt{\varepsilon}$ as a function of both the angular radius θ and the absolute radius r. For the numerical evaluation of $n_{\mathrm{H}}\sqrt{\varepsilon}$ from $I(\mathrm{H}\beta)$, we have used the functions defined in the appendix of Harrington & Feibelman (1983). The coefficients, defined there, which yield the functions shown in Figs 2(a) and 7 are $k=2$, $n=25$, $h_1=0.043$, $h_2=0.076$, $a'_{1,25}=1.0$, $a'_{2,25}=0.32$, all other $a'_{k,n}=0$, and $N_0=3.3\times10^{-9}\,\mathrm{cm}^{-3}$. For the evaluation of $n_{\mathrm{H}}\sqrt{\varepsilon}$ we adopted an observed $F(\mathrm{H}\beta)=1.70\times10^{-13}\,\mathrm{erg\,cm^{-2}\,s^{-1}}$, from the fluxes measured by Osmer (1976) and Webster (1983). We adopted a reddening of $E(B-V)=0.06$, corresponding to $E(B-V)=0.02$ by galactic foreground reddening (McNamara & Feltz 1980) plus $E(B-V)=0.04$ from dust within the SMC (Caldwell & Coulson 1985). The dereddened Hβ flux is thus $I(\mathrm{H}\beta)=2.07\times10^{-13}\,\mathrm{erg\,cm^{-2}\,s^{-1}}$. We used $T_{\mathrm{e}}=13\,400$ K, the [O III] electron temperature from the work of Aller *et al.* (1981), for the evaluation of $\alpha_{\mathrm{eff}}(\mathrm{H}\beta)$. From their results we also obtained $\gamma=1.13$. Finally, we adopted a distance of 57.5 kpc for the SMC, corresponding to a distance modulus of 18.8 (Rich, Da Costa & Mould 1984; Reid & Strugnell 1986).

The mass of the ionized nebula is given by

$$M(\mathrm{PN})=\mu m_{\mathrm{H}}\int \varepsilon n_{\mathrm{H}}(r)4\pi r^2\,dr$$

$$=4\pi\mu m_{\mathrm{H}}\sqrt{\varepsilon}\int n_{\mathrm{H}}(r)\sqrt{\varepsilon}r^2\,dr, \tag{5}$$

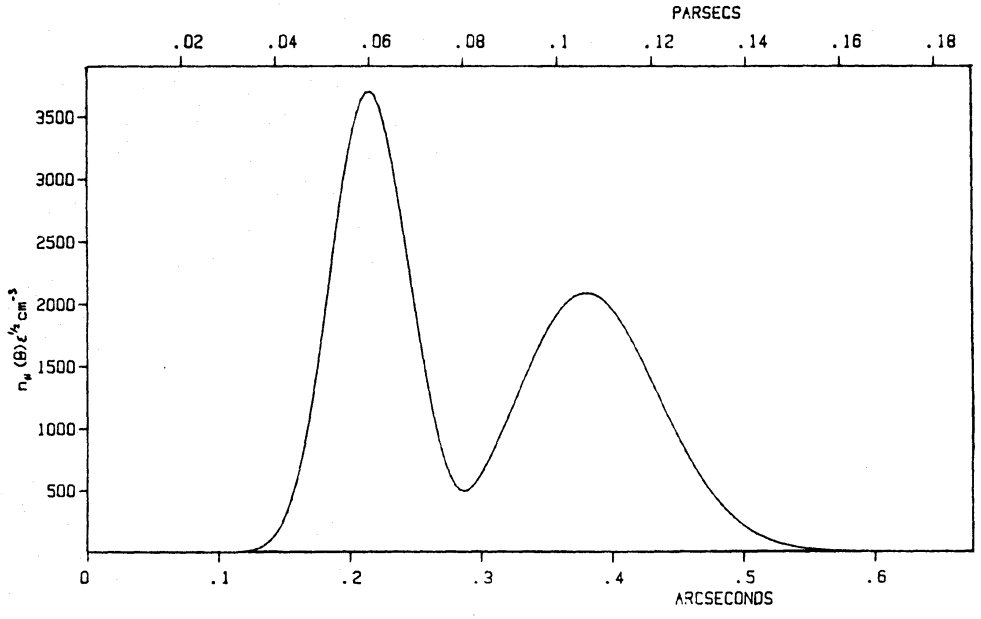

Figure 7. A plot of the derived density distribution of SMC N2, $n_{\mathrm{H}}\varepsilon^{1/2}$ (see text), as a function of angular radius (lower abscissa) and absolute radius (upper abscissa).

where m_H is the mass of a hydrogen atom and $\mu=[1+4n(\mathrm{He})/n(\mathrm{H})]$. The results of Aller *et al.* (1981) yield $\mu=1.43$ for SMC N2. We have numerically evaluated the integral in (5) to obtain

$$M(\mathrm{PN})=0.53\sqrt{\varepsilon}M_\odot. \tag{6}$$

We find that 76 per cent of the mass (versus 64 per cent of the emission) is located in the outer shell.

In order to determine the nebular mass, it now remains to derive the value of the filling factor for SMC N2. To do this we have made use of observations of the electron-density-sensitive [O II] 3726, 3729 Å doublet ratio. The mean nebular electron density $\langle n_e\rangle$ yielded by this ratio is a measure of the local electron density in the nebula averaged over the entire nebula. In a manner similar to equation (3) of Harrington & Feibelman (1983), we can write

$$\langle n_e\rangle=\frac{\int n_e\varepsilon n_i r^2\,dr}{\int \varepsilon n_i r^2\,dr}. \tag{7}$$

This can be written as

$$\langle n_e\rangle\sqrt{\varepsilon}=\gamma\,\frac{\int n_H^2\varepsilon r^2\,dr}{\int n_H\varepsilon^{1/2}r^2\,dr} \tag{8}$$

if we assume that the filling factor is the same throughout the nebula and that O^+ has the same radial distribution in the nebula as H^+. Since we know $n_H\sqrt{\varepsilon}$ as a function of r (Fig. 7), we can evaluate the integral in (8). We obtain $\langle n_e\rangle\sqrt{\varepsilon}=1970\,\mathrm{cm}^{-3}$. The value of $\langle n_e\rangle$ for SMC N2 was derived from the [O II] doublet ratio which was measured as part of PATT service observations at the AAT on 1985 January 4 of a number of Magellanic Cloud PN (Barlow & Walsh, in preparation). The 3726.0/3728.7 line intensity ratio was found to be 1.69, in agreement with the value of 1.7 measured by Webster (1976). A ratio of 1.69, in conjunction with an electron temperature of 13 400 K, gives $\langle n_e\rangle=2850\,\mathrm{cm}^{-3}$, using the collision strengths of Pradhan (1976) and the transition probabilities of Zeippen (1982). Thus we obtain $\varepsilon=0.48$ and $M(\mathrm{PN})=0.37\,M_\odot$, when assuming that O^+ has the same distribution as H^+. A better estimate of ε can be obtained from an ionization structure model constructed to reproduce the observed absolute emission-line fluxes from SMC N2. Such a model is described in the Appendix, where it is shown that the observed [O II] 3726/3729 ratio of 1.69 implies $\varepsilon=0.45$.

We therefore have for SMC N2

$$\varepsilon=0.45$$

$$M(\mathrm{PN})=0.36\,M_\odot. \tag{9}$$

The inner nebular shell contains $0.09\,M_\odot$, while the outer shell contains $0.27\,M_\odot$.

We now consider how sensitive the derived nebular mass is to uncertainties in the input parameters and assumptions.

(i) Our speckle observations are fitted by a double-ring structure. We have made the standard

assumption that these rings correspond to spherical shells seen in projection on the sky. We may also consider the case where the observed rings are instead due to tori whose planes happen to lie perpendicular to our line-of-sight. Such structures might arise, for example, as a result of equatorial rather than spherical ejection by the central star. If ω is the solid angle occupied by the tori, as seen from the central star, then we may repeat the previous analysis by substituting ω for 4π on the right-hand side of equation (1). Equation (2) is unchanged, while the right-hand side of equation (3) is multiplied by $\omega/4\pi$. Since the other parameters are unchanged, the value of K derived from equation (3) will be a factor of $\omega/4\pi$ smaller than for the spherical case and $n_{\rm H}(r)\sqrt{\varepsilon}$, given by equation (4), will be a factor of $(4\pi/\omega)^{1/2}$ larger. Since its numerator is fixed by the Hβ flux, equation (8) implies that $\langle n_{\rm e}\rangle\sqrt{\varepsilon}$ changes by the inverse of the product of $\omega/4\pi$ and $n_{\rm H}(r)\sqrt{\varepsilon}$, i.e. $\langle n_{\rm e}\rangle\sqrt{\varepsilon}$ is proportional to $(4\pi/\omega)^{1/2}$. Since $\langle n_{\rm e}\rangle$ is fixed by the [O II] observations, this implies that the value of $n_{\rm H}(r)$ is the same for both the spherical shell and the torus cases, and that only ε changes, being proportional to $4\pi/\omega$. Since the filling factor ε cannot exceed unity and since the spherical case gave $\varepsilon=0.45$, we see that the smallest covered fraction of the sky that is allowed for the torus case is equal to 0.45. The mass of the PN for the torus case is given by equation (5) with a reduction in the solid angle from 4π to ω, which is exactly balanced by the increase in ε by $4\pi/\omega$. The derived nebular mass is therefore the same for both geometries.

(ii) The quantities best determined by the speckle observations are the angular radii of the radial intensity peaks shown in Fig. 2(a). With these radii fixed, we have investigated the effects of varying the widths and relative intensities of the two peaks. The nebular mass given by equation (5) is proportional to the product of $\sqrt{\varepsilon}$ and the integral of $\sqrt{\varepsilon}n_{\rm H}(r)r^2\,dr$. The former quantity is given by equation (8) which, for a fixed Hβ flux, has a fixed numerator, from equation (1). We can therefore substitute for $\sqrt{\varepsilon}$ from equation (8) into equation (5), to see that M(PN) is invariant for a fixed value of $\langle n_{\rm e}\rangle$. For example, when the FWHM's of the radial intensity peaks in Fig. 2(a) are both increased by 25 per cent, the autocorrelation that results is smoother and gives a significantly poorer fit to the observed speckle component in Fig. 2(b), while the derived filling factor decreases from 0.45 to 0.36, and the total nebular mass remains unchanged. If, on the other hand, the ratio of the areas of the two radial intensity peaks is changed from the value of 2.2 shown in Fig. 2(a) to 1.0 (i.e. identical peaks but unchanged positions), the autocorrelation that results gives a significantly poorer fit to the speckle component in Fig. 2(b), the derived filling factor increases to 0.64, but the derived nebular mass is again unchanged.

(iii) The derived nebular mass is also insensitive to the radii of the intensity peaks. From equations (3) and (4), changing the radii by a factor of y leads to a change $y^{-3/2}$ in $n_{\rm H}\sqrt{\varepsilon}$ at the new radius yr, relative to the previous value of $n_{\rm H}\sqrt{\varepsilon}$ at radius r. The integral of $n_{\rm H}\varepsilon^{1/2}r^2\,dr$ therefore changes by a factor of $y^3/y^{3/2}$. Since the numerator of equation (8) is unchanged, the value of $\sqrt{\varepsilon}$ changes by $y^{-3/2}$. Because the terms outside and inside the integral in equation (5) for the nebular mass change by factors of $y^{-3/2}$ and $y^{3/2}$, the nebular mass remains the same. This result holds even if the radii of the two peaks are changed by different factors. However, the radii of the shells cannot be reduced by more than 30 per cent or else the derived filling factor will exceed unity. Our observations in fact constrain the radii of the peaks of the shells to ± 6 per cent.

(iv) Finally, the formal uncertainty of ± 0.08, from counting statistics, for our [O II] doublet ratio translates into an uncertainty of ± 15 per cent in the derived nebula mass.

We conclude that it is primarily the filling factor ε which is sensitive to the uncertainties in our fitting procedures, our best estimate for ε being 0.45. The total nebular mass, on the other hand, is surprisingly insensitive to these uncertainties. The uncertainty in the distance modulus of the SMC is probably the most important source of error in the mass estimate. As discussed in Section 1, a distance modulus uncertainty of ± 0.3 mag translates into a mass uncertainty of ± 30 per cent, giving us $M(\mathrm{PN})=0.36\pm 0.12\,M_{\odot}$ for SMC N2.

5 The expansion age of SMC N2

Having determined an absolute radius for SMC N2, we are in a position to derive an expansion age for the nebula from its measured expansion velocity. The spectrum illustrated in Fig. 8 is the profile of the [O III] 5007 Å line emitted by SMC N2. It was obtained for us by Dr J. Meaburn using the University of Manchester Echelle Spectrometer (Meaburn *et al.* 1984) on the AAT. The projected slit width was 1 arcsec and the exposure time was 350 s. The instrumental resolution, as determined from the FWHM of comparison arc lines, was 12.9 km s^{-1}. The observed profile of the [O III] line in Fig. 8 is due to a convolution of the intrinsic line profile with the instrumental profile, so the FWHM of 36.9 km s^{-1} found for the observed profile using a single Gaussian fit (dashed curve in Fig. 8) implies an intrinsic line profile FWHM of 34.6 km s^{-1} after deconvolution. We may attribute the observed profile to a superposition of the effects of the expansion of the nebula along with the thermal line broadening. The latter depends on the mass of the ion and for T_e(O III)=13 400 K the predicted thermal line broadening corresponds to a Gaussian with a FWHM of 6.1 km s^{-1}. After deconvolution we thus obtain a FWHM of 34.1 km s^{-1} which can be attributed to the effects of nebular expansion alone. Robinson *et al.* (1982) have shown that a spherically symmetric nebula with an expansion velocity proportional to radius (as seems to be implied by data on other PN, see below) will yield a line profile whose FWHM is nearly equal to twice the nebular expansion velocity at the radius of peak emission, if the nebula is observed with an aperture larger than the nebular diameter. On this basis we derive an expansion velocity of 17 km s^{-1} which, with the outer shell radius of 0.105 pc derived in Section 4, implies an expansion age of 6000 yr for SMC N2, provided the velocity has been constant with time.

Since our speckle observations have shown that SMC N2 possesses two shells, we have also fitted the observed [O III] profile with two Gaussians, whose relative intensities, central positions and FWHM's were allowed to vary until the residuals between the observed and computed profiles were minimized (to do this we used the line fitting program ELF, written by Dr P. J. Storey, within the STARLINK package DIPSO of Howarth & Maslen 1984). The best fit was obtained with components which were offset by 4 km s^{-1} and whose FWHM's were 29.6 and

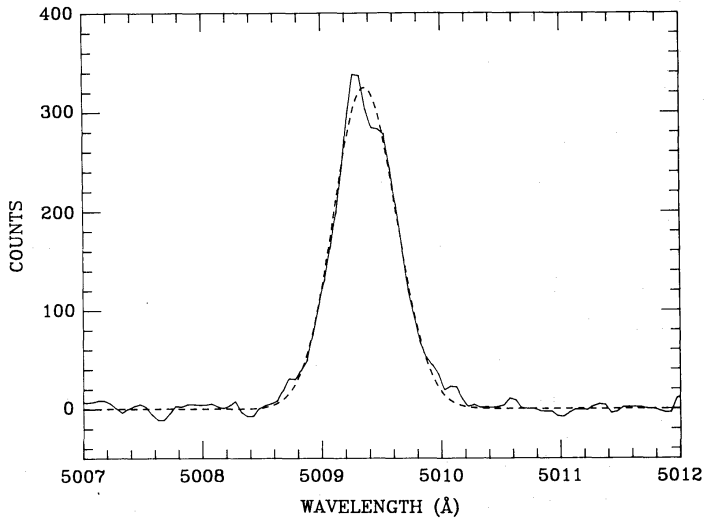

Figure 8. The profile of the [O III] 5007 Å line emitted by SMC N2, obtained with the University of Manchester Echelle Spectrometer on 1983 November 17 (see text). The dashed curve shows a single-Gaussian fit to the observed profile and has a FWHM of 36.9 km s^{-1}. The centroid of the Gaussian fit yields a heliocentric radial velocity of +164.8 km s^{-1} for SMC N2.

44.1 km s^{-1}, respectively contributing 42 and 58 per cent of the total emission. After correction for the effects of instrumental and thermal line broadening, these widths translate into expansion velocities of 13 and 20.8 km s^{-1} for the two components. Since our speckle results (Section 4) gave similar relative intensities for the inner and outer nebular shells (36 and 64 per cent), we respectively identify the lower and higher expansion velocities with the inner and outer shells. This identification is supported by the fact that the ratio of the expansion velocities of the two components is nearly equal to the ratio of the radii of the two shells – velocity mappings of many galactic PN have shown that the expansion velocity within a nebula usually increases linearly with angular radius (Osterbrock 1974, p. 156).

Observational studies (e.g. Smith 1971; Robinson, Reay & Atherton 1982) have also shown that for a sample of galactic PN with some assumed common distance scale, the measured expansion velocity for each PN appears to be proportional to its absolute outer nebular radius. We can derive expansion ages for the two shells of SMC N2 on the basis of this model if we assume that each shell was initially ejected with the same constant expansion velocity, u, and thereafter attained a velocity at radius r given by $v(r)=u+k(r-R)$, where k is a constant (different for each shell) and R is the radius at which acceleration first occurred [$v(r)=u$ for $r\leqslant R$]. If we adopt $u=10$ km s^{-1}, representative of AGB wind expansion velocities (Knapp & Morris 1985), we derive expansion ages of 5000 and 7000 yr for the inner and outer shells, respectively, if we assume that both shells started accelerating at $r=R=0$. If we assume that both shells started accelerating at the time that the second shell was ejected then we derive expansion ages of 5000 and 8000 yr for the inner and outer shells. If we adopt an initial velocity of $u=5$ km s^{-1}, which is at the lower end of measured AGB wind expansion velocities, then the assumption of acceleration starting at $r=0$ leads to ages of 7000 and 9000 yr for the inner and outer shells, while the assumption that the acceleration commenced when the second shell was ejected leads to ages of 7000 and 12 000 yr for the two shells. Finally, the assumption that the outer shell at 0.105 pc has always had its current expansion velocity of 20.8 km s^{-1} leads to a lower limit of 5000 yr for the expansion age of the nebula, while constant velocity expansion of the 0.06 pc radius inner shell at its current velocity of 13 km s^{-1} would imply a minimum expansion age of 4500 yr.

6 Discussion

SMC N2 is one of three Magellanic Cloud PN for which Stecher *et al.* (1982) derived stellar luminosities, from *IUE* data, which were close to the theoretical maximum for core masses below the Chandrasekhar limit. For SMC N2, the central star mass of 0.9 $M_{\odot}$, which they obtained from their derived luminosity of 33 000 $L_{\odot}$, is so high that the time-scale for a decline of the initial stellar luminosity by a factor of 10 should only be a few hundred years ($T\propto M^{-9.6}$, Iben & Renzini 1983). Such a time-scale is incompatible with the nebular expansion age of greater than 5000 yr which is implied by our data. Tylenda (1984) has also argued, on independent grounds, that the stellar luminosities and masses were overestimated by Stecher *et al.*

In the Appendix we describe how we have analysed the available data on SMC N2 in order to derive the nebular ionization structure and the central star parameters. We used the Stoy energy balance method, and the stellar He II Lyman continuum photon flux implied by the nebular He II 4686 Å recombination line flux, in order to define the range of allowable central star temperatures and luminosities, and then constructed nebular ionization structure models using the code described by Harrington *et al.* (1982), so as to find the best-fitting case. We found that no stellar blackbody model could satisfy the observations. The best-fitting model was produced by a central star with an NLTE energy distribution corresponding to $T_{\rm eff}=110\,000$ K and $\log g=5.75$, and a luminosity of 4340 $L_{\odot}$. Neglecting distance modulus uncertainties, the uncertainty in the derived luminosity is $\pm 400\,L_{\odot}$. Our derived luminosity of 4340 $L_{\odot}$ is a factor of 7.6 smaller than

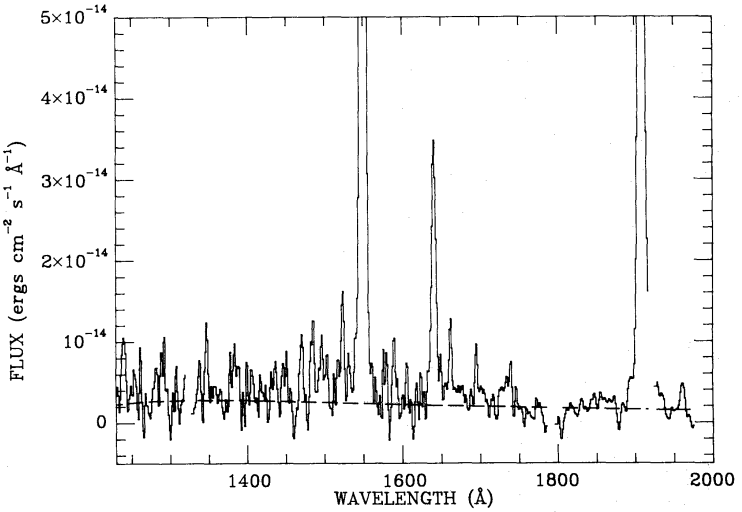

Figure 9. The observed *IUE* low-resolution spectrum of SMC N2, formed by merging the spectra from SWP 20454 and SWP 20527. Gaps in the spectrum indicate the positions of reseaux. The dashed curve shows the predicted reddened continuum, formed by adding the theoretical nebular continuum to the continuum of the NLTE stellar model which provides the best fit to the nebular observations (see Appendix).

that derived by Stecher *et al.*, of which only a factor of 1.3 can be attributed to the slightly smaller distance modulus adopted here. We attribute most of the discrepancy to the fact that Stecher *et al.*'s luminosity was based on a He II Zanstra temperature determination at 1640 Å. As is apparent from Fig. 9, the continuum signal-to-noise level in the *IUE* SWP spectra of SMC N2 is sufficiently low that very large uncertainties can arise from this method.

The central star mass can be derived by plotting its luminosity and temperature on an H–R diagram and interpolating between the central star evolutionary tracks which have been published for a range of core masses. Interpolation between the hydrogen-burning tracks calculated by Schönberner (1981, 1983) yielded a central star mass of $0.593\,M_{\odot}$ and an evolutionary age since $T_{\rm eff}$ was equal to 5000 K of 8100 yr. A comparison with the hydrogen-burning tracks calculated by Wood & Faulkner (1984) yielded a central star mass of $0.60\,M_{\odot}$ and an evolutionary age since $T_{\rm eff}$ was equal to 10 000 K of about 12 000 yr. The alternative Wood & Faulkner case of PN ejection during a helium shell flash, followed by evolution while helium-burning, gives a central star mass of 0.64–$0.65\,M_{\odot}$ and an evolutionary age of only 3000 yr. The L, $T_{\rm eff}$ position of SMC N2 implies that it has reached the high-temperature edge of its evolutionary track and begun to slowly decline in luminosity, so that the Paczynski (1971) relation for steady hydrogen-shell burning cannot be used to derive the core mass. The luminosity just after leaving the AGB would have been $M_{\rm bol}=-4.65$ for a $0.593\,M_{\odot}$ core, according to the Schönberner hydrogen-burning evolutionary tracks, and $M_{\rm bol}=-5.2$ according to the Wood & Faulkner helium-burning tracks. The hydrogen-burning central star evolutionary age of 8000–12 000 yr since leaving the AGB region is compatible with the nebular expansion ages derived in Section 5, whereas the helium-burning evolutionary age of 3000 yr is uncomfortably short compared to the minimum nebular expansion age of 5000 yr estimated in Section 5.

Our derived mass of $0.59\,M_{\odot}$ and radius of $0.181\,R_{\odot}$ for the central star of SMC N2 imply an effective gravity corresponding to $\log g=5.7$, consistent with the central star surface gravity of $\log g=5.75$ used for our nebular ionization structure modelling (Appendix). The C/O abundance ratio found from our nebular ionization structure modelling was 4.5 ± 1 (Maran *et al.* 1982 found C/O=2). Maran *et al.* concluded that the AGB progenitor was a Carbon star, but the luminosity

of $M_{bol}=-6.6$ which Stecher *et al.* (1982) derived for the central star was considerably brighter than the highest luminosity found for Magellanic Cloud Carbon stars: $M_{bol}=-6$ (e.g. Cohen *et al.* 1981; Wood, Bessell & Fox 1983; Iben 1984). The initial luminosity of $M_{bol}=-4.7$ to -5.2 derived here for SMC N2 instead puts it squarely within the $M_{bol}=-4$ to -6 range found for Magellanic Cloud Carbon stars. The derived luminosity is insensitive to the assumed radial structure of the nebula, although both the present luminosity, and that of Stecher *et al.* (1982), are based on the assumption of a spherically symmetric nebula. In the event of a toroidal geometry, our analysis in Section 4 showed that the smallest fraction of the sky that could be occupied by the nebula, as seen from the star, is 0.45. The maximum stellar luminosity for the case of toroidal geometry is therefore $4340/0.45=9640\,L_{\odot}$ ($M_{bol}=-5.2$), corresponding to a core mass of $0.67\,M_{\odot}$ for hydrogen-burning and an evolutionary age of 2000 yr. Since this is significantly shorter than the minimum nebular expansion age and since the increase in stellar luminosity would lead to a higher degree of ionization in the nebula than observed, we prefer the results of the spherically symmetric analysis.

An AGB progenitor star mass of about $1\,M_{\odot}$ is implied by the hydrogen-burning stellar core mass of $0.59\,M_{\odot}$ and the nebular shell mass of $0.36\,M_{\odot}$ which we have derived. The shell mass is significantly larger than the $0.11\,M_{\odot}$ predicted for a $0.59\,M_{\odot}$ core by Wood *et al.* (1983) from their derivation of AGB star pulsational masses assuming first overtone pulsation and core masses assuming hydrogen-shell burning. Their analysis did predict a shell mass of $0.36\,M_{\odot}$ for a hydrogen-shell burning core mass at the tip of the AGB of $0.64\,M_{\odot}$, which, if the star had since switched to helium-shell burning, would be consistent with our nebular mass of $0.36\,M_{\odot}$ and our core mass of $0.64\,M_{\odot}$ derived for the case of helium-burning. However, as discussed above, the helium-burning stellar evolutionary age of 3000 yr is rather short compared to the minimum nebular expansion age of 5000 yr or the most likely expansion age of 8000 yr. Another possibility comes from the alternative analysis by Wood *et al.* of their AGB star data for the case of fundamental mode pulsation (and hydrogen-shell burning as before). This yielded a total pulsational mass of just under $1.0\,M_{\odot}$ for a core mass of $0.60\,M_{\odot}$, i.e. a shell mass of about $0.4\,M_{\odot}$, which appears to be consistent with our results. Their analysis predicts that a small change in core mass should be accompanied by a large change in shell mass, so it will be of interest to see if this is confirmed by the extension of the type of analysis presented here to a larger sample of planetary nebulae.

Acknowledgments

We thank Dr John Meaburn for obtaining the [O III] spectrum of SMC N2 for us and for the loan of the 5007 Å filter. We also thank Dr Ken Reay for the loan of the Hβ filter and Dr Neill Reid for discussions of the distance scale for the Magellanic Clouds. We are particularly grateful to Dr Robin Clegg for the use of his programmes and unpublished data. We are grateful to Dr J. P. Harrington for the use of his nebular photoionization code. We acknowledge an award of AAT time by PATT and we would like to thank Dr Jeremy Walsh for obtaining the [O II] spectrum for us during AAT PATT service time. We also thank David Monk for help with the preparation of the paper. This work has been generously supported by the SERC and in particular CS is grateful for a SERC studentship and an ICI grant, and HV for SERC support as an Assistant Research Officer.

References

Aller, L. H., Keyes, C. D., Ross, J. E. & O'Mara, B. J., 1981. *Mon. Not. R. astr. Soc.*, **194,** 613.
Atherton, P. D., Hicks, T. R., Reay, N. K., Worswick, S. P. & Hayden Smith, W., 1978. *Astr. Astrophys.*, **66,** 297.

Auer, L. H. & Mihalas, D., 1972. *Astrophys. J. Suppl.,* **24,** 193.
Barker, T., 1983. *Astrophys. J.,* **267,** 630.
Brocklehurst, M., 1971. *Mon. Not. R. astr. Soc.,* **153,** 471.
Caldwell, J. A. R. & Coulson, I. M., 1985. *Mon. Not. R. astr. Soc.,* **212,** 879.
Clegg, R. E. S., Harrington, J. P., Barlow, M. J. & Walsh, J. R., 1986. *Astrophys. J.,* submitted.
Cobb, M. L. & McCarthy, E. W., 1986. *SPIE Proc. Vol. 627, Instrumentation in Astronomy VI.*
Cohen, J. G., Frogel, J. A., Persson, S. E. & Elias, J. H., 1981. *Astrophys. J.,* **249,** 481.
Gathier, R., Pottasch, S. R., Goss, W. M. & Van Gorkom, J. H., 1983. *Astr. Astrophys.,* **128,** 325.
Harrington, J. P., Seaton, M. J., Adams, S. & Lutz, J. H., 1982. *Mon. Not. R. astr. Soc.,* **199,** 517.
Harrington, J. P. & Feibelman, W. A., 1983. *Astrophys. J.,* **265,** 258.
Hebden, J. C., Morgan, B. L. & Vine, H., 1983. *Proc. Soc. Photo-opt. Instr. Eng.,* **445,** 477.
Henize, K. G., 1956. *Astrophys. J. Suppl.,* **2,** 315.
Howarth, I. D., 1983. *Mon. Not. R. astr. Soc.,* **203,** 301.
Howarth, I. D. & Maslen, D., 1984. *Starlink User Note 50.*
Iben, I. Jr, 1984. *Observational Tests of the Stellar Evolution Theory, IAU Symp. No. 105,* p. 3, eds Maeder, A. & Renzini, A., Reidel, Dordrecht, Holland.
Iben, I. Jr & Renzini, A., 1983. *Ann. Rev. Astr. Astrophys.,* **21,** 271.
Jacoby, G. H., 1980. *Astrophys. J. Suppl.,* **42,** 1.
Knapp, G. R. & Morris, M., 1985. *Astrophys. J.,* **292,** 640.
Maran, S. P., Aller, L. H., Gull, T. R. & Stecher, T. P., 1982. *Astrophys. J.,* **253,** L43.
McNamara, D. H. & Feltz, K. A. Jr, 1980. *Publs astr. Soc. Pacif.,* **92,** 587.
Mendoza, C., 1983. *Planetary Nebulae, IAU Symp. No. 103,* p. 143, ed. Flower, D. R., Reidel, Dordrecht, Holland.
Meaburn, J., Blundell, B., Carling, R., Gregory, D. F., Keir, D. & Wynne, C. G., 1984. *Mon. Not. R. astr. Soc.,* **210,** 463.
Osmer, P., 1976. *Astrophys. J.,* **203,** 352.
Osterbrock, D. E., 1974. *Astrophysics of Gaseous Nebulae,* W. H. Freeman, San Francisco.
Paczynski, B., 1971. *Acta Astr.,* **21,** 417.
Pradhan, A. K., 1976. *Mon. Not. R. astr. Soc.,* **177,** 31.
Preite-Martinez, A. & Pottasch, S. R., 1983. *Astr. Astrophys.,* **126,** 31.
Reid, N. & Strugnell, P., 1986. *Mon. Not. R. astr. Soc.,* in press.
Rich, R. M., Da Costa, F. S. & Mould, J. R., 1984. *Astrophys. J.,* **286,** 517.
Robinson, G. J., Reay, N. K. & Atherton, P. D., 1982. *Mon. Not. R. astr. Soc.,* **199,** 649.
Roddier, F., 1981. *Prog. Opts,* **19,** 281.
Schönberner, D., 1981. *Astr. Astrophys.,* **103,** 119.
Schönberner, D., 1983. *Astrophys. J.,* **272,** 708.
Seaquist, E. R. & Davis, L. E., 1983. *Astrophys. J.,* **274,** 659.
Shaw, R. A. & Kaler, J. B., 1985. *Astrophys. J.,* **295,** 537.
Smith, H. Jr, 1971. *Astr. J.,* **76,** 193.
Stecher, T. P., Maran, S. P., Gull, T. R., Aller, L. H. & Savedoff, M. P., 1982. *Astrophys. J.,* **262,** L41.
Tylenda, R., 1984. *Astr. Astrophys.,* **138,** 317.
Webster, B. L., 1969. *Mon. Not. R. astr. Soc.,* **143,** 79.
Webster, B. L., 1976. *Mon. Not. R. astr. Soc.,* **174,** 513.
Webster, B. L., 1983. *Publs astr. Soc. Pacif.,* **95,** 610.
Wood, P. R., Bessell, M. S. & Fox, M. W., 1983. *Astrophys. J.,* **272,** 99.
Wood, P. R. & Faulkner, D. J., 1984. *Observational Tests of the Steller Evolution Theory,* p. 179, eds Maeder, A. & Renzini, A., Reidel, Dordrecht, Holland.
Zeippen, C. J., 1982. *Mon. Not. R. astr. Soc.,* **198,** 111.

Appendix: An ionization structure model for SMC N2

In order to determine more accurately the filling factor in SMC N2, and thus the nebular mass, and secondly to determine the central star parameters, we have produced a spherically symmetric ionization structure model for the nebula using the code written by Dr J. P. Harrington (see Harrington *et al.* 1982, and Clegg *et al.* 1986 for a description) and implemented on the UCL STARLINK node by Dr R. E. S. Clegg.

Column 3 of Table A1 lists the relative intensities of the emission lines which have been observed from SMC N2, on a scale where Hβ=100. The fluxes of the lines between 1200 and 2000 Å were obtained from the merged *IUE* spectrum resulting from SWP 20454 (100 min) and SWP 20527 (90 min). These images, from the programme of Maran *et al.*, were obtained from the *IUE* data-bank. The fluxes of the lines between 3000 and 4000 Å were obtained from the AAT service spectrum of Barlow & Walsh, described in Section 4, while the fluxes of the lines longwards of 4000 Å are from Aller *et al.* (1981). The [Ne v] 3426 Å line is blended with the O III 3429 Å Bowen line, with about one half of the total flux estimated to be due to [Ne v]. As discussed in Section 4, we have adopted a total extinction of $E(B-V)=0.06$ to SMC N2, with $E(B-V)=0.02$ due to foreground galactic extinction and $E(B-V)=0.04$ due to extinction within

Table A1. Observed, dereddened and model fluxes for SMC N2.

Ion	λ(Å)	Observed	Dered.	Model(ϵ=0.45)
OIV	1401	<40	<58	3.2
CIV	1549	929	1293	989
HeII	1640	139.4	189.4	198.0
CIII]	1908	753	993	1290
[NeV],OIII	3426,29	7.2	7.6(NeV 3.8)	2.4(NeV)
[OII]	3726	17.5	18.7	18.9
[OII]	3729	10.4	11.1	11.2
[NeIII]	3868	70.5	74.4	73.1
[NeIII]	3967	20.1	21.0	22.6
[OIII]	4363	12.8	13.1	13.1
HeI	4471	3.7	3.8	4.0
HeII	4686	28.4	28.6	28.3
Hβ	4861	100	100	100
[OIII]	4959	297	296	297
[OIII]	5007	(855)	(853)	854
HeI	5876	11.5	11.1	10.5
[SIII]	6312	0.8	0.8	0.8
Hα	6563	310	292	288
[NII]	6584	8.8	8.3	8.3
[SII]	6717,31	4.0	3.8	1.1
[OII]	7325	5.3	4.9	2.6

Nebular abundances relative to hydrogen (by number):

He : 0.109
C : 6.75×10^{-4}
N : 2.00×10^{-5}
O : 1.48×10^{-4}
Ne : 2.60×10^{-5}
S : 1.90×10^{-6}

the SMC. Column 4 of Table A1 lists the dereddened relative line intensities, where we have assumed that the fit to the LMC reddening law presented by Howarth (1983) provides a reasonable approximation to the less well determined SMC extinction law. Inspection of Table A1 shows that with this dereddening the relative intensities of He II $\lambda\lambda$1640 and 4686 are consistent with the theoretical ratio (Column 5).

The starting values of the elemental abundances used in the models were derived from an empirical analysis of the dereddened line intensities. For this we adopted T_e=13 400 K, the [O III] electron temperature, and n_e=2850 cm^{-3}, the [O II] electron density (Section 4) along with the collision strengths tabulated by Mendoza (1983) and the empirical ionization correction factors listed by Barker (1983). We obtained the following abundances (by number relative to hydrogen): He:0.109; C:6.5×10^{-4}; N:2.7×10^{-5}; O:1.75×10^{-4}; Ne:2.6×10^{-5}; and S:2.0×10^{-6}.

In order to determine the parameters of the central star, we used the Stoy energy-balance method as developed by Preite-Martinez & Pottasch (1983). The available dereddened line intensities give ϱ=36.0, where ϱ is the ratio of the flux in collisionally excited lines to the flux in the Hβ recombination line. To this we added a contribution of ϱ=5.7 from unobserved collisionally excited lines (e.g. C III 977 Å, He I 10830 Å, and the infrared fine structure lines), which we derived by normalizing the predicted relative intensities of observed and unobserved lines from the same ion to the fluxes of the observed lines. For the case of a central star with a blackbody energy distribution, the final value of ϱ=41.7 implies an effective temperature of 128 000 K. Case II of Preite-Martinez & Pottasch (1983) was assumed, corresponding to a nebula which is optically thick in the He II Lyman continuum and optically thin in the hydrogen Lyman continuum (these assumptions are supported by the observed He^+/He^{2+} ratio of 3.4 and were confirmed by the ionization structure modelling). The stellar radius is given by the requirement that the star emit the number of He II Lyman continuum photons implied by the nebular He II 4686 Å flux. For a distance of 57.5 kpc, the dereddened He II 4686 Å flux of 5.92×10^{-14} erg cm^{-2} s^{-1} yields $4\pi R_*^2 N(He^+)$=2.64×10^{46} s^{-1}, the total number of photons emitted by the star shortwards of 228 Å. A blackbody temperature of 128 000 K implies a stellar radius of 0.112 $R_\odot$ and a luminosity of 3030 $L_\odot$.

The nebular radial density distribution that was used in the ionization structure modelling is that shown in Fig. 7, with the filling factor ε as a free parameter to be derived. It was found that a blackbody model was unable to maintain the observed degree of ionization in the nebula, for any value of the filling factor. The ratio of the predicted line fluxes from low-ionization stages to those from higher ionization stages was much larger than observed. By lowering the blackbody stellar temperature, the overall stellar luminosity required to provide the He II ionizing flux could be raised, thereby increasing the degree of ionization in the nebula, but such models then produced values for the electron temperature and ϱ which were too low.

We therefore turned to NLTE stellar energy distributions to power the nebula. Because of the energy redistribution around the He II edge at 228 Å, NLTE atmospheres can produce more nebular heating (higher ϱ) than blackbodies of the same temperature, since relatively more stellar photons are emitted just longwards of 228 Å, producing significant heating after ionizing hydrogen, and fewer photons are available for ionizing He^+. In order to supply the same number of He II Lyman continuum photons as a blackbody giving the same value of ϱ, an NLTE model atmosphere with a He II absorption edge must be more luminous, and so a higher degree of ionization in the nebula can be expected.

A grid of Auer & Mihalas (1972) hydrogen and helium blanketed NLTE model-atmosphere energy distributions, calculated on the University of London CRAY-1S, have been analysed (Clegg, work to be published) in order to obtain the appropriate values of χ, the energy gain coefficients defined by Preite-Martinez & Pottasch (1983); along with values for $N(He^+)$ and

N(H), the fluxes of stellar photons emitted per unit surface area shortwards of 228 and 912 Å, respectively. Grids of increasing $T_{\rm eff}$ were calculated for several values of $\log g$, all models having $n({\rm He})/n({\rm H})=0.1$. It was found that the observed ϱ of 41.7 required an NLTE effective temperature in the region of 110 000 K, the exact value being a function of surface gravity.

In order to derive the appropriate gravity for the central star of SMC N2, we have made use of the following technique, which relies on the known distance of the nebula. The stellar radius and effective temperature which are required at a given $\log g$ in order to give the correct He II Lyman continuum flux, determine the stellar luminosity. The luminosity and the effective temperature can be used to derive the stellar mass, by comparison with theoretical evolutionary tracks such as those of Schönberner (1981, 1983). The surface gravity implied by this mass and by the stellar radius can then be checked for consistency with the surface gravity of the model atmosphere. As an example, an NLTE model atmosphere with $T_{\rm eff}=110\,000$ K and $\log g=6.5$ would require a stellar radius of $0.28\,R_\odot$ in order to maintain the nebular He II ionization in SMC N2. The resulting luminosity of $10^4\,L_\odot$ and the effective temperature imply a stellar mass of $0.675\,M_\odot$. This mass and the stellar radius of $0.28\,R_\odot$ give $\log g=5.4$, inconsistent with the $\log g=6.5$ of the model atmosphere. As the surface gravity of a model atmosphere is lowered and the He II 228 Å absorption jump decreases, the stellar radius required for the necessary He II ionizing flux also decreases. When $T_{\rm eff}=110\,000$ K and $\log g=5.7$, the required stellar radius is $0.176\,R_\odot$, yielding a luminosity of $4095\,L_\odot$, a stellar mass of $0.59\,M_\odot$ and $\log g=5.73$, which is consistent with the surface gravity of the model atmosphere. In order to test the validity of this technique, we have calculated a grid of nebular ionization structure models for SMC N2 using central stars with NLTE effective temperatures ranging from 100 000 to 130 000 K and $\log g$'s ranging from 5.2 to 6.7. The model atmosphere which produced the best fit to the observed $T_{\rm e}$(O III) and ϱ, and to the observed level of ionization in the nebula, had $T_{\rm eff}=110\,000$ K and $\log g=5.75$. The required stellar radius was $0.181\,R_\odot$ and so the stellar luminosity was $4340\,L_\odot$. The effective temperature and the luminosity give a stellar mass of $0.593\,M_\odot$, upon comparison with the Schonberner evolutionary tracks, and the radius and mass give $\log g=5.69$, consistent with the surface gravity of the model atmosphere.

This model atmosphere energy distribution and luminosity was used for our nebular ionization structure modelling, with the elemental abundances and the filling factor as adjustable parameters. As mentioned earlier, the radial hydrogen density distribution that was used is that shown in Fig. 7. Our philosophy for judging the goodness of fit of a model to the observations was to try to match, (i) the fluxes of the electron-temperature-sensitive [O III] lines $\lambda\lambda$4363, 4959, 5007; (ii) the fluxes of the electron-density-sensitive [O II] 3726 and 3729 Å lines; and (iii) the total flux in the strong coolant lines of C IV 1549 Å and C III] 1908 Å. The final values of the O and C abundances were determined by (i) and (ii), respectively, while the final N, Ne and S abundances were those that gave the best fits to the fluxes in [N II] λ6584, [Ne III] $\lambda\lambda$3868, 3967 and [S III] λ6312, respectively. The final abundances are listed at the foot of Table 1 and are close to the starting values obtained from the empirical abundance analysis.

It was found that although the overall flux in the [O II] $\lambda\lambda$3726, 3729 lines was sensitive to the stellar luminosity, the 3726/3729 flux *ratio* was sensitive only to the filling factor ε. The observed 3726/3729 ratio was matched by $\varepsilon=0.45$. Column 5 of Table A1 lists the predicted relative fluxes from our final best-fit model with $\varepsilon=0.45$. The main discrepancy with the observations exhibited by the final model is that the predicted fluxes in C IV λ1549 and C III] λ1908 are respectively 30 per cent too low and 30 per cent too high, although their combined cooling flux is equal to that observed. Models with the inner nebular hole (Fig. 7) filled to a maximum density of 40 per cent of that at the peak of the inner shell, as allowed by the speckle observations, produced no significant changes in the predicted fluxes since very little mass is contained in the central regions. A nebular model with $\varepsilon=1.0$ produced the correct ratio of C IV λ1549 to C III] λ1908, since

the lower mean density implied by a higher filling factor gave a higher degree of ionization in the nebula. However, the 3726/3729 ratio of 1.43 predicted by the $\varepsilon=1.0$ model was inconsistent with the observed ratio of 1.69, while the overall [O II] 3726, 3729 Å flux was a factor of 2 too low.

The nebular mass corresponding to the best-fit model with $\varepsilon=0.45$ is 0.36 $M_{\odot}$ and the nebula is optically thin in the hydrogen Lyman continuum. The unreddened apparent central star magnitude at V (5500 Å) is predicted to be 21.4, while the unreddened stellar flux at 1308 Å is predicted to be 2.25×10^{-15} erg cm^{-2} s^{-1} Å^{-1}. In Fig. 9 we have plotted the *observed* 1200–2000 Å spectrum of SMC N2, which results from merging SWP 20454 and SWP 20527. The spectra were extracted using the STARLINK package IUEDR, written by J. R. Giddings. Also plotted in Fig. 9 is the continuum which results from reddening the sum of the theoretical nebular continuum and the model central star continuum. The galactic and SMC extinctions and reddening laws which were used are those described at the beginning of the Appendix. It can be seen that there is satisfactory agreement between the predicted and observed continuum levels.